Conditional quantum-state engineering using ancillary squeezed-vacuum states

Hyunseok Jeong,[1] Andrew M. Lance,[2] Nicolai B. Grosse,[2] Thomas Symul,[2] Ping Koy Lam,[2] and Timothy C. Ralph[1]

[1]*Department of Physics, University of Queensland, St Lucia, Queensland 4072, Australia*
[2]*Quantum Optics Group, Department of Physics, Faculty of Science, Australian National University, ACT 0200, Australia*

We investigate an optical scheme to conditionally engineer quantum states using a beam splitter, homodyne detection, and a squeezed vacuum as an ancillar state. This scheme is efficient in producing non-Gaussian quantum states such as squeezed single photons and superpositions of coherent states (SCSs). We show that a SCS with well defined parity and high fidelity can be generated from a Fock state of $n \leq 4$, and conjecture that this can be generalized for an arbitrary n Fock state. We describe our experimental demonstration of this scheme using coherent input states and measuring experimental fidelities that are only achievable using quantum resources.

I. INTRODUCTION

Quantum state engineering using measurement induced conditional evolution is an important and useful technique in the field of quantum optics and quantum information processing [1]. It is known that a near deterministic, universal set of unitary transformations can be achieved for qubit systems using this principle [2,3], and that arbitrary optical states can be engineered conditionally based on discrete single photon measurements [4]. Recently, there has been increased interest in conditional evolution based on continuous-variable measurements [5–8]. In these schemes a quantum system is interacted with a prepared ancilla, which is measured via a continuous observable, e.g., a quadrature variable of the electromagnetic field. This has been experimentally demonstrated for a system using a beam splitter as the interaction and a vacuum state as the ancilla with conditioning based on homodyne detection to remotely prepare a qubit state [7]. A similar system using conditioning of adaptive phase measurements has also been discussed [8].

Recently, an optical scheme was suggested to engineer interesting continuous-variable non-Gaussian quantum states based on a beam-splitter interaction, using an ancilla squeezed vacuum state and conditioning homodyne detection [9]. It is a difficult task to generate and engineer non-Gaussian continuous-variable quantum states in optical fields. For example, a superposition of free-traveling coherent states (SCS) is very hard to generate in spite of its potential usefulness for quantum information processing [10] and fundamental interest in relation to the quantum superposition ("Schrödinger's cat") paradox [11]. As another example, it is highly nontrivial to directly squeeze a single photon in a squeezing apparatus, even though the squeezed single photon can also be useful for quantum information processing applications [12–16]. The scheme in Ref. [9] enables one to conditionally squeeze a single photon with an arbitrarily high fidelity using the squeezed vacuum of any finite degree of squeezing. It also enables one to transform a two-photon state into a SCS with an extremely high fidelity. The principles of the postselection scheme were experimentally demonstrated using coherent states, and experimental fidelities were measured that are only achievable using quantum resources [9].

In this paper, we develop the scheme presented in Ref. [9] and fully describe its experimental demonstration. In particular, we find that a SCS with well defined parity and high fidelity can be generated from a Fock state of $n \leq 4$, and conjecture that this can be generalized for an arbitrary n. We also compare the postselection scheme [9] with another scheme based on the feedforward method using the displacement operation [17]. It is known that the squeezing operation for an arbitrary input state can be approximately performed using the highly squeezed vacuum as an ancillar, a beam splitter, and the feedforward method with the displacement operation [17]. However, the interesting features of the postselection scheme that we described above for non-Gaussian inputs cannot be achieved using the feedforward method in Ref. [17]. This shows that quantum state engineering using postselection is an interesting tool for quantum information processing. On the other hand, for Gaussian coherent states, the standard feedforward scheme can be modified to perform the same transformation with the postselection scheme. In this case, the postselection scheme can be understood as an alternative method to the feedforward scheme [17,18].

II. ENGINEERING VARIOUS INPUT STATES USING A SQUEEZED VACUUM AND POSTSELECTION

Our conditional transformation scheme is depicted in Fig. 1. The squeezed vacuum used as the ancilla state in our scheme is represented as $\hat{S}(s)|0\rangle$ with the squeezing operator $\hat{S}(s) = \exp[-(s/2)(\hat{a}^2 - \hat{a}^{\dagger 2})]$, where s is the squeezing parameter and $\hat{a}$ is the annihilation operator. The Wigner function of the squeezed vacuum is

$$W_{\text{sqz}}(\alpha; s) = \frac{2}{\pi} \exp[-2(\alpha^+)^2 e^{-2s} - 2(\alpha^-)^2 e^{2s}], \quad (1)$$

where $\alpha = \alpha^+ + i\alpha^-$ with real quadrature variables α^+ and α^-. The first step of our transformation protocol is to interfere the input field with the ancilla state on a beam splitter as shown in Fig. 1(a). The beam-splitter operator $\hat{B}$ acting on modes $\hat{a}$ and $\hat{b}$ is represented as
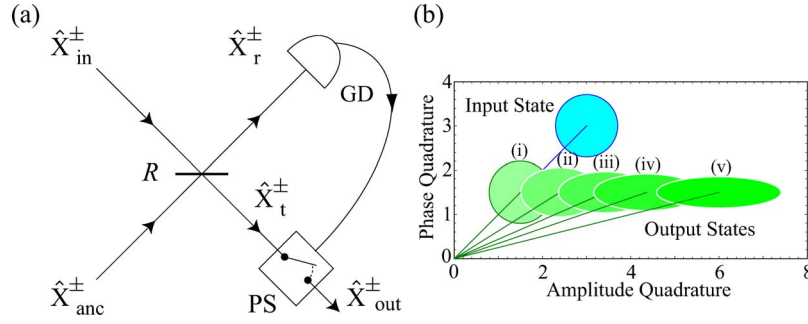
FIG. 1. (Color online) (a) Schematic of the post-selection protocol. $\hat{X}_{in}^{\pm}$: amplitude $(+)$ and phase $(-)$ quadratures of the input state; anc: ancilla squeezed vacuum state; r: reflected; t: transmitted; out: post-selected output state. R: beam-splitter reflectivity; GD: gate detector; PS: post-selection protocol. (b) Standard deviation contours of the Wigner functions of an input coherent state (blue) and post-selected output states (green) for $R=0.75$ and varying ancilla state squeezing of (i) $s=0$, (ii) $s=0.35$, (iii) $s=0.69$, (iv) $s=1.03$, and (v) ideal squeezing.

$$\hat{B}(\theta) = \exp\left\{\frac{\theta}{2}(\hat{a}^{\dagger}\hat{b} - \hat{b}^{\dagger}\hat{a})\right\}, \qquad (2)$$

where the reflectivity is defined as $R=\sin^2(\theta/2)$ and where $T=1-R$. A homodyne measurement is performed on the amplitude quadrature on the reflected field mode, with the measurement result denoted as X_r^+. The transmitted state is post-selected for $|X_r^+|<x_0$, where the postselection threshold x_0 is determined by the required fidelity between the output state and the ideal target state. As we will see later in this section, the postselection process in our scheme plays a crucial role in engineering non-Gaussian states with finite squeezing resources.

A. Squeezing a single photon

We first consider a single-photon state input $|1\rangle$ and a squeezed single photon $\hat{S}(s')|1\rangle$ as the target state. The Wigner function of the single photon state is

$$W_{in}^{|1\rangle}(\alpha) = \frac{2}{\pi}\exp[-2|\alpha|^2](4|\alpha|^2 - 1). \qquad (3)$$

After interference via the beam splitter, the resulting two-mode state becomes

$$W^{(1)}(\alpha,\beta) = W_{in}^{|1\rangle}(\sqrt{T}\alpha + \sqrt{R}\beta)W_{anc}(-\sqrt{R}\alpha + \sqrt{T}\beta), \qquad (4)$$

where $W_{anc} = W_{sqz}(\alpha;s)$ and $\beta=\beta^+ + i\beta^-$. Note that the superscript (1) indicates that the input state was the single-photon Fock state. We will use this notation (n) for various quantities throughout the paper to denote that the input state was the n-photon Fock state. The transmitted state after the homodyne detection of the reflected state is

$$W_{out}^{(1)}(\alpha;X_r^+) = P_{(1)}(X_r^+)^{-1}\int_{-\infty}^{\infty}d\beta^- W^{(1)}(\alpha,\beta^+ = X_r^+,\beta^-), \qquad (5)$$

where the normalization parameter is

$$P_{(1)}(X_r^+) = \int_{-\infty}^{\infty}d^2\alpha d\beta^- W^{(1)}(\alpha,\beta^+ = X_r^+,\beta^-)$$

$$= \frac{2e^{-s-2X_r^{+2}/(R+Te^{2s})}(T^2e^{4s} + e^{2s}TR + 4RX_r^{+2})}{\pi(R+Te^{2s})^2\sqrt{T+e^{-2s}}}. \qquad (6)$$

If the measurement result is $X_r^+=0$, the Wigner function of the output state becomes

$$W_{out}^{(1)}(X_r^+ = 0;\alpha) = \frac{2}{\pi}e^{-2[e^{-2s'}(\alpha^+)^2 + e^{2s'}(\alpha^-)^2]}\{4e^{-2s'}(\alpha^+)^2$$

$$+ 4e^{2s'}(\alpha^-)^2 - 1\} \equiv W_{SSP}(\alpha), \qquad (7)$$

where

$$s' = -\frac{1}{2}\ln[T + e^{-2s}R]. \qquad (8)$$

One can immediately notice that the output state in Eq. (7) is exactly the Wigner function $W_{ssp}(\alpha)$ of a squeezed single photon $\hat{S}(s')|1\rangle$. We note that the output squeezing s' can be arbitrarily close to the squeezing of the ancilla state s by making R close to zero.

For a nonzero postselection threshold criteria $|X_r^+|<x_0$ the corresponding success probability is given by

$$\mathcal{P}_s^{(1)}(x_0) = \int_{-x_0}^{x_0}dX_r^+ P_{(1)}(X_r^+) \qquad (9)$$

and the average Wigner function $W_{ave}^{(1)}(\alpha;x_0)$ is

$$W_{ave}^{(1)}(\alpha;x_0) = \frac{\displaystyle\int_{-x_0}^{x_0}dX_r^+ P_{(1)}(X_r^+)W_{out}^{(1)}(\alpha,X_r^+)}{\displaystyle\int_{-x_0}^{x_0}d\tilde{X}_r^+ P_{(1)}(\tilde{X}_r^+)}. \qquad (10)$$

The fidelity between the output state (with the measurement result X_r^+) and the ideal target state is obtained as
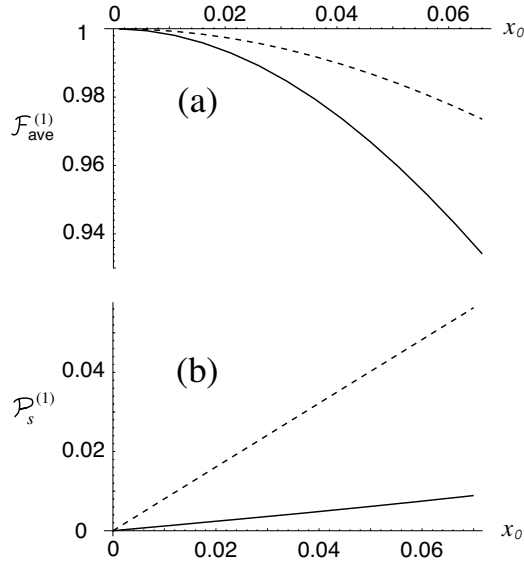
FIG. 2. (a) The average fidelity $\mathcal{F}_{\text{ave}}^{(1)}$ between the post-selected output state of an input single photon state $|1\rangle$ and the ideal squeezed single photon target state $\hat{S}(s')|1\rangle$. (b) The success probability $\mathcal{P}_s^{(1)}$ against the post-selection threshold x_0. Solid line: beam-splitter reflectivity $R=0.98$, ancillary state squeezing $s=0.7$, and target state squeezing of $s'=0.67$. Dashed line: beam-splitter reflectivity of $R=0.5$, ancillary state squeezing $s=-0.7$, and target state squeezing of $s=-0.464$.

$$\mathcal{F}_{(1)}(X_r^+) = \pi \int_{-\infty}^{\infty} d^2\alpha\, W_{\text{out}}^{(1)}(\alpha;X_r^+)\, W_{\text{SSP}}(\alpha). \qquad (11)$$

The average fidelity of the output state for a postselection threshold x_0 is

$$\mathcal{F}_{\text{ave}}^{(1)}(x_0) = \frac{\displaystyle\int_{-x_0}^{x_0} dX_r^+\, P_{(1)}(X_r^+)\, \mathcal{F}_{(1)}(X_r^+)}{\displaystyle\int_{-x_0}^{x_0} d\widetilde{X}_r^+\, P_{(1)}(\widetilde{X}_r^+)}. \qquad (12)$$

Alternatively, the average fidelity for a threshold x_0 can be obtained using the average Wigner function as

$$\mathcal{F}_{\text{ave}}^{(1)}(x_0) = \pi \int_{-\infty}^{\infty} d^2\alpha\, W_{\text{ave}}^{(1)}(\alpha;x_0)\, W_{\text{SSP}}(\alpha). \qquad (13)$$

We use this average fidelity measure to characterize the efficacy of our protocol for nonzero thresholds.

The average fidelity $\mathcal{F}_{\text{ave}}^{(1)}$ and success probability $\mathcal{P}_s^{(1)}$ have been plotted for a couple of cases in Fig. 2. Suppose that the ancillar squeezing is $s=0.7$ (6.08 dB phase squeezing) with the beam splitter ratio $R=0.98$ and the postselection threshold is $x_0=0.025$. Then, the output squeezing is $s'=0.67$ (5.82 dB) and the average fidelity is $\mathcal{F}_{\text{ave}}^{(1)}=0.99$ with the success probability $\mathcal{P}_s^{(1)}=0.003$. As another example, if $s=-0.7$ (6.08 dB amplitude squeezing) and $x_0=0.04$ with $R=1/2$ are assumed, the results are $s'=-0.464$ (4.03 dB) and $\mathcal{F}_{\text{ave}}^{(1)}=0.99$ with $\mathcal{P}_s^{(1)}=0.016$. The average Wigner functions corresponding to an average fidel-
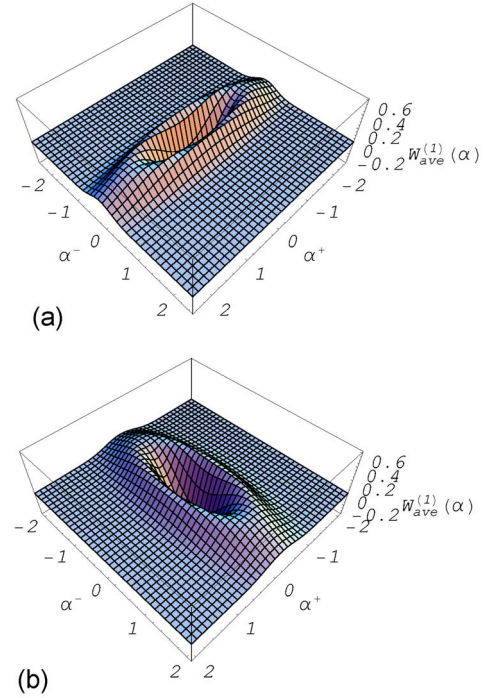

FIG. 3. (Color online) The average Wigner function $W_{\text{ave}}^{(1)}(\alpha)$ of the output state corresponding to $\mathcal{F}_{\text{ave}}^{(1)}=0.99$ (a) for $x_0=0.025$, $R=0.98$, $s=0.7$, and $\mathcal{P}_s^{(1)}=0.003$ and for (b) $x_0=0.04$, $R=1/2$, $s=-0.7$, and $\mathcal{P}_s^{(1)}=0.016$.

ity $\mathcal{F}_{\text{ave}}^{(1)}=0.99$ for these cases are shown in Fig. 3.

We emphasize that squeezing a single photon using the squeezed vacuum with such high fidelities and high degrees of the output squeezing *cannot* be achieved by the feedforward method [17] unless the ancillar squeezing becomes extremely high (which is not realistic). However, our scheme enables one to perform this interesting task with any finite degree of the ancillar squeezing. Figure 4 shows that the output states obtained by the feedforward method are distorted but the postselection for an appropriate threshold results in the desired state. Figure 5 explains the role of the postselection for a non-Gaussian input: if the homodyne result X^+ is far from zero, the shape of the output state become distorted, i.e., the output state loses the non-Gaussian characteristics. Therefore, it cannot be corrected by the feedforward with any electronic gain, and the postselection is necessary to select non-Gaussian output states. In other words, postselection around $X_r^+=0$ preserves the non-Gaussian features of the input state.

B. Converting Fock states to superposition of coherent states

We now examine Fock states for $n \geq 2$ as input states. Our target states are the SCSs

$$|\text{SCS}_\pm\rangle = \frac{1}{\sqrt{2 \pm 2e^{-2|\gamma|^2}}}(|\gamma\rangle \pm |-\gamma\rangle), \qquad (14)$$

where $|\gamma\rangle$ is a coherent state of amplitude $\gamma=\gamma^+ + i\gamma^-$. The SCSs are often referred to as "Schrödinger cat states" due to
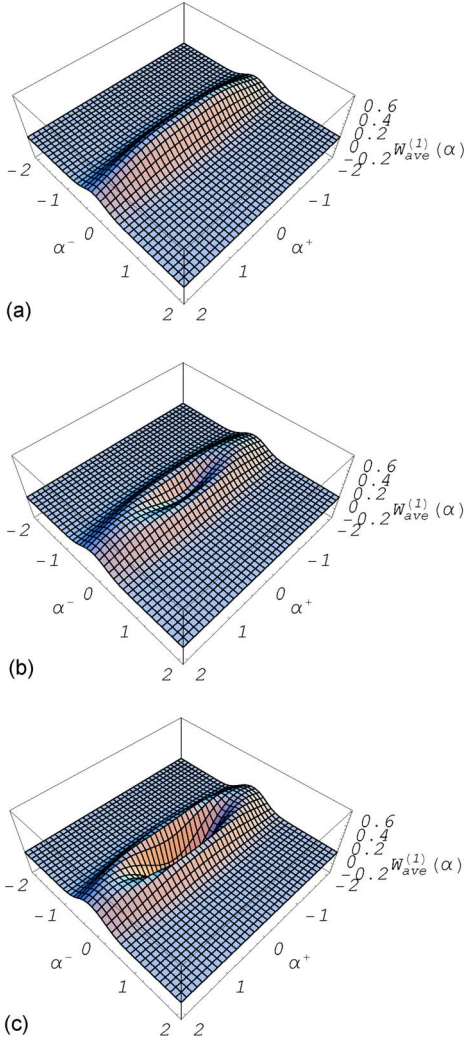
(a)

(b)

(c)

FIG. 4. (Color online) (a) The average Wigner function $W_{ave}^{(1)}$ $\times(\alpha)$ of the output state obtained from the single-photon input with $s=0.7$ and $R=0.98$ using the feedforward scheme with the unity gain. The non-Gaussian quantum characteristics are washed away. (b) If the result obtained by the feedforward method is postselected for $x=0.3$, the non-Gaussian characteristic begins to emerge. (c) The average fidelity $\mathcal{F}_{ave}^{(1)}=0.87$ and the minimum negative value $W_{ave}^{(1)}(0)\approx-0.48$ are obtained for threshold $x_0=0.1$.
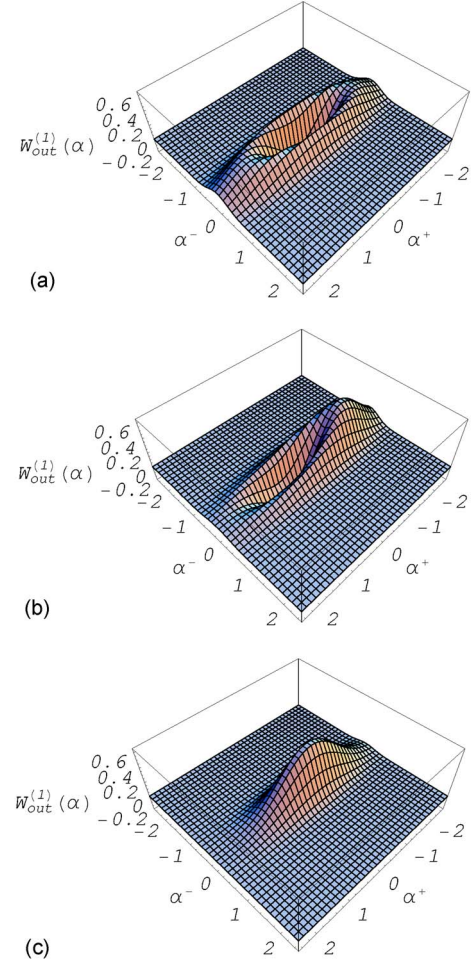

(a)

(b)

(c)

FIG. 5. (Color online) The Wigner function $W_{out}^{(1)}(\alpha)$ of the output state obtained from the single-photon input with $s=0.7$ and $R=0.98$. (a) If the measurement result is $X_r^+=0$, an ideal squeezed single photon with $s'=0.67$ is obtained, i.e., the fidelity is $\mathcal{F}_{(1)}(X_r^+$ $=0)=1$. However, the non-Gaussian shape is distorted as the measurement results deviate from zero as (b) $\mathcal{F}_{(1)}(X_r^+=-0.1)=0.67$ and (c) $\mathcal{F}_{(1)}(X_r^+=-0.5)=0.03$. The non-Gaussian characteristics cannot be recovered by the classical feedforward methods after such distortions. It is clear from this figure that the postselection is necessary to preserve the non-Gaussian feature for the output state.

their characteristics as superpositions of macroscopically distinguishable states. The SCSs $|SCS_+\rangle$ and $|SCS_-\rangle$ are called even and odd SCSs, respectively. The even SCS contains only even number of photons and becomes the vacuum as the amplitude goes to zero, i.e., $\alpha \to 0$. On the other hand, the odd SCS contains only odd number of photons and approaches the single photon state $|1\rangle$ as the amplitude goes to zero. The Wigner representations of the even and odd SCSs are

$$W_{SCS}^{\pm}(\alpha) = N_{\pm}\{e^{-2|\alpha-\gamma|^2} + e^{-2|\alpha+\gamma|^2} \pm e^{-2|\gamma|^2}$$

$$\times(e^{-2(\alpha+\gamma)^*(\alpha-\gamma)} + e^{-2(\alpha+\gamma)(\alpha-\gamma)^*})\}, \quad (15)$$

where $N_{\pm}=\{\pi(1\pm e^{-2|\gamma|^2})\}^{-1}$. In this subsection, we shall as-

sume γ to be pure imaginary for simplicity of equations without losing generality.

The output Wigner function, average fidelity and success probability can be obtained in the same way described in Eqs. (4)–(13). The Wigner function of the output state for the two-photon input with the measurement result X_r^+ and the beam-splitter reflectivity $R=1/2$ is given by

$$W_{out}^{(2)}(\alpha;X_r^+) = N_2 e^{-G}\{1 + 2Z + (3 + 16\alpha_i^2)Z^2 + (4 - 16\alpha_i^2)Z^3$$

$$+ (2 - 32\alpha_i^2 + 64\alpha_i^4)Z^4 + 4\alpha_r'^4(1 + Z)^4$$

$$- 4\alpha_r'^2(1 + Z)^2[1 + 3Z + (2 - 8\alpha_i^2)Z]\}, \quad (16)$$

where $G=2\alpha_i^2+\alpha_r'^2+Z^{-1}(\alpha_r-X^+)^2+2\alpha_i^2\tanh[s]$, $\alpha_r'=\alpha_r+X^+$,
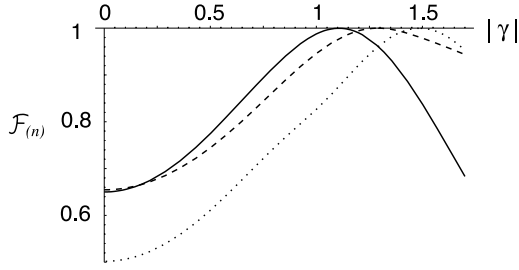
FIG. 6. The fidelity $\mathcal{F}_{(n)}$ between the ideal SCSs $W_{SCS}^{\pm}(\alpha)$ with amplitude $|\gamma|$ and the output states $W_{out}^{(n)}(\alpha; X_r^+ = 0)$ from the n-photon input Fock states for $n=2$ (solid line), $n=3$ (dashed line), and $n=4$ (dotted line). Note that the target state is the ideal even (odd) SCS when n is an even (odd) number.

$Z = e^{2s}$, and N_2 is the normalization factor. The success probability is $\mathcal{P}_s^{(2)}(x_0) = \int_{-x_0}^{x_0} dX_r^+ P_{(2)}(X_r^+)$ with

$$P_{(2)}(X_r^+) = \frac{J e^{-s - 4X_r^{+2}/K}}{\sqrt{\pi(1 + e^{-2s})J^4}}, \qquad (17)$$

where $J = 4e^{6s} + 2e^{8s} + (1 - 8X_r^{+2})^2 + 2e^{2s}(1 + 8X_r^{+2}) + e^{4s}(3 + 32X_r^{+2})$ and $K = 1 + e^{2s}$. The fidelity is calculated as $\mathcal{F}_{(2)} \times (X_r^+) = \pi \int_{-\infty}^{\infty} d^2\alpha W_{out}^{(2)}(\alpha; X_r^+) W_{SCS}^+(\alpha)$. If the measurement result is $X_r^+ = 0$ with $R = 1/2$, the fidelity between the ideal *even* SCS in Eq. (15) and the output state (16) is simplified as

$$\mathcal{F}_{(2)}(X_r^+ = 0) = \frac{A K^{5/2}[1 + 4e^{2s} + (3 - 8\gamma^2)e^{4s}]^2}{(1 + e^{2\gamma^2})(1 + 3e^{2s})^5(1 + 2e^{4s})}, \quad (18)$$

where $A = 4\sqrt{2}\exp[\gamma^2 + s + \gamma^2 \sinh s/(2\cosh s) + \sinh s]$. If the ancillar squeezing is $s = -0.37$ (3.21 dB), the fidelity becomes $\mathcal{F}_{(2)}(X_r^+ = 0) \approx 0.9997$ for $\gamma = 1.1i$, i.e., a SCS of amplitude $|\gamma| = 1.1$ with extremely high fidelity can be obtained from a two-photon Fock state using the squeezed vacuum of 3.21 dB squeezing.

Our calculation can be extended for the cases of $n=3$ and $n=4$. We have obtained the fidelity between the output state $W_{out}^{(3)}(\alpha)$ and the ideal odd SCS for $X_r^+ = 0$ as

$$\mathcal{F}_{(3)}(X_r^+ = 0) = \frac{4\gamma^2 e^{2s} A K^{7/2} L^2 (\coth \gamma^2 - 1)}{3(3 + 2e^{4s})(1 + 3e^{2s})^7}, \quad (19)$$

where $L = 3 + 12e^{2s} + (9 - 8\gamma^2)e^{4s}$. The even state is the target state for $n=4$, and in this case the fidelity for $X_r^+ = 0$ is

$$\mathcal{F}_{(4)}(X_r^+ = 0) = \frac{A K^{9/2} M^2}{3(1 + e^{2\gamma^2})(1 + 3e^{2s})^9(3 + 24e^{4s} + 8e^{8s})} \quad (20)$$

with $M = 3 + 24e^{2s} + (66 - 48\gamma^2)e^{4s} - 24(8\gamma^2 - 3)e^{6s} + (64\gamma^4 - 144\gamma^2 + 27)e^{8s}$. The fidelities (18)–(20) for the maximized squeezed parameter, i.e., $\max_s \mathcal{F}_{(n)}(X = 0)$, have been plotted for amplitude γ of the SCSs in Fig. 6. It shows that the fidelity becomes close to one, for a given number n, when the squeezed parameter and the amplitude are properly optimized. One can find the amplitude of the cat state that maximizes the fidelity for a given number n. The maximum fidelity $\mathcal{F}_{(2)} = 0.9997$ is obtained when $s = -0.37$ (2.95 dB)
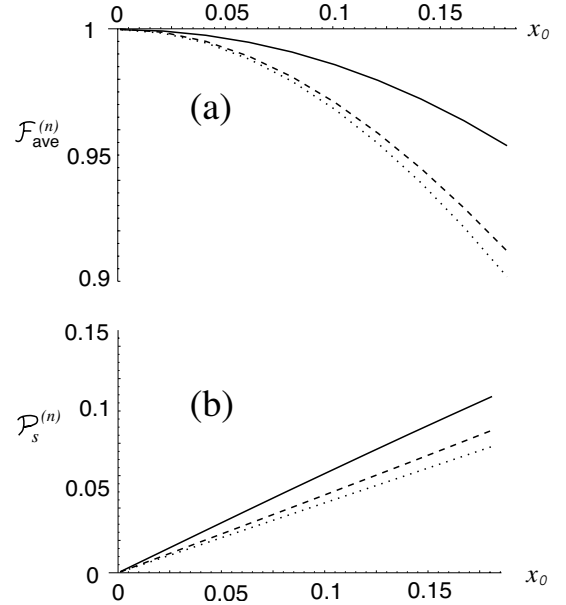

FIG. 7. (a) The average fidelity $\mathcal{F}_{ave}^{(n)}$ between the ideal SCS and the output state of the input Fock state $|n\rangle$ and (b) the success probability $\mathcal{P}_s^{(n)}$ for varying threshold x_0. The beam splitter reflectivity is $R = 1/2$. Solid line: $n=2$, the ancillar squeezing is $s = -0.37$, and the amplitude of the target SCS is $|\gamma| = 1.1$. Dashed line: $n=3$, the ancillar squeezing is $s = -0.34$, and the amplitude of the target SCS is $|\gamma| = 1.29$. Dotted line: $n=4$, the ancillar squeezing is $s = -0.37$, and the amplitude of the target SCS is $|\gamma| = 1.49$.

and $\alpha = 1.1i$. The same result $\mathcal{F}_{(3)} = 0.9999$ ($\mathcal{F}_{(4)} = 0.9997$) can be obtained for $n=3$ ($n=4$) when $s = -0.34$ ($s = -0.37$) and $\alpha = 1.29i$ ($\alpha = 1.49i$).

We have calculated the success probability $\mathcal{P}_s^{(n)}(x_0)$ and the average fidelity $\mathcal{F}_{ave}^{(n)}$ for $n=2$ to $n=4$ as described above and plotted for varying threshold x_0 in Fig. 7. Our numerical calculations show that $\mathcal{F}_{ave}^{(2)} = 0.999$ is obtained for 1.4% when $X_0 = 0.022$ for the two-photon input state, and $\mathcal{F}_{ave}^{(3)} = 0.999$ ($\mathcal{F}_{ave}^{(4)} = 0.999$) is obtained for 0.8% (0.6%) when $X_0 = 0.017$ ($X_0 = 0.014$). The success probability is improved if the required fidelity is $\mathcal{F}_{ave}^{(n)} = 0.99$. Using the same conditions, $\mathcal{F}_{ave}^{(2)} = 0.99$ is obtained for 5.2% when $X_0 = 0.084$. The same fidelity $\mathcal{F}_{ave}^{(3)} = 0.99$ ($\mathcal{F}_{ave}^{(4)} = 0.99$) is obtained for 2.8% (2.4%) when $X_0 = 0.058$ ($X_0 = 0.055$). In Fig. 8, the average output Wigner functions $W_{ave}^{(n)}$ for the input n-photon Fock states look identical to the Wigner functions of the corresponding even and odd SCSs due to the high fidelities (=0.99).

Based on our results, we can conjecture that an n-photon Fock state can be converted to an SCS using our scheme, and the parity of the SCS is determined by the parity of the input Fock state. It will be interesting to prove our conjecture for an arbitrary number n, which is yet beyond the scope of our paper.

C. Squeezing coherent states

We now consider the case of a Gaussian state, i.e., an unknown coherent state $|\gamma\rangle$ as the input. The postselection
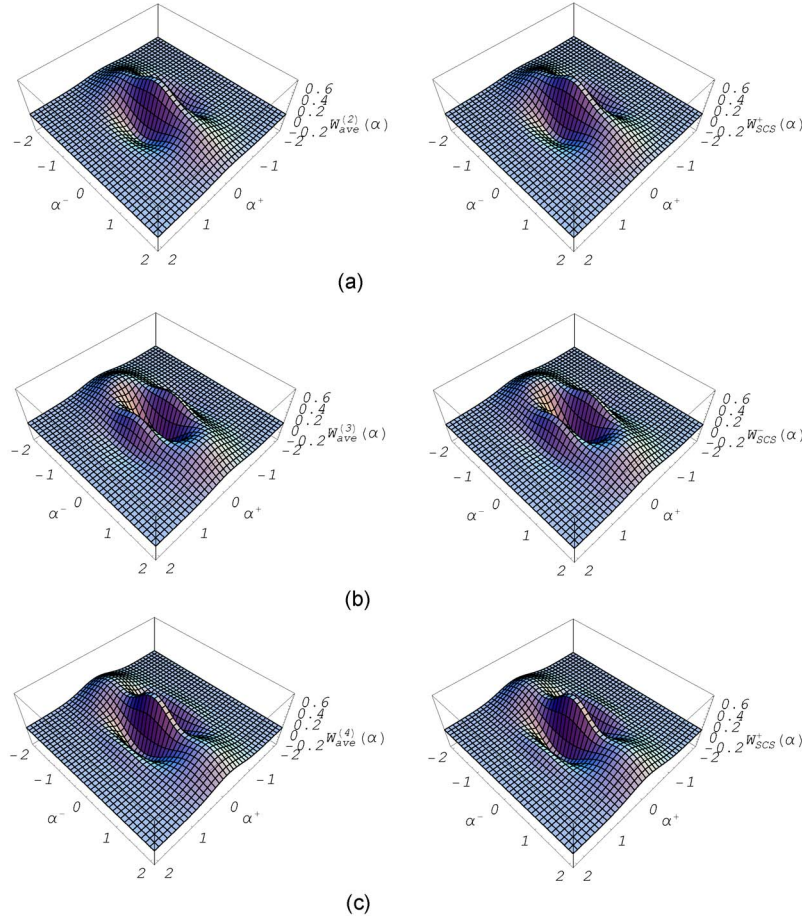
FIG. 8. (Color online) The average Wigner functions $W_{\text{ave}}^{(n)}$ of the output state corresponding to $\mathcal{F}_{\text{ave}}^{(n)}=0.99$ for (a) $n=2$, $x_0=0.084$, and $\mathcal{P}_s^{(2)}=0.055$, for (b) $n=3$, $x_0=0.0583$, and $\mathcal{P}_s^{(3)}=0.0309$, and for (c) $n=4$, $x_0=0.0555$, and $\mathcal{P}_s^{(4)}=0.0254$. It is clearly observed that the average output Wigner functions (left-hand side) are virtually identical to those of ideal even ($n=2,4$) and odd ($n=3$) SCSs (right-hand side) with the corresponding amplitudes.

scheme for $X_r^+=0$ transforms the coherent state as

$$D(\gamma)|0\rangle \rightarrow D(\sqrt{T}[e^{2s'}\gamma^+ + i\gamma^-])S(s')|0\rangle, \quad (21)$$

where $D(\gamma)=\exp[\gamma\hat{a}^\dagger - \gamma^*\hat{a}]$ is the displacement operator and the output squeezing s' is

$$s' = -\frac{1}{2}\ln[T + e^{-2s}R] \quad (22)$$

with the ancillar squeezing s. These relations can be obtained by analyzing the input and output Wigner functions. Note that Eq. (22) for coherent state inputs is identical to Eq. (8) for single photon inputs. The transform in Eq. (21), illustrated in Fig. 1(b), has an interesting property in that it preserves the purity of the input coherent state, i.e., the output is a minimum uncertainty state, independent of the amount of squeezing of the ancilla state. In the ideal limit of perfect phase squeezing of the ancilla state $s\rightarrow\infty$, the post-selection scheme works as an ideal single-mode squeezer for arbitrary input coherent states $D(\gamma)|0\rangle \rightarrow S(s')D(\gamma)|0\rangle$. In this case, the output squeezing is $s'\rightarrow -\ln[T]/2$. On the other hand, if $s<0$, s' is not limited by the beam splitter ratio while the

transformation does not work as an ideal squeezer in the limit of the infinite squeezing.

It is interesting to note that the transformation (21) using the postselection scheme outperforms the feedforward scheme with the standard gain [17] to squeeze unknown coherent states for small amplitudes as shown in Fig. 9. The standard gain for the feedforward scheme is

$$g = \sqrt{\frac{R}{T}} \quad (23)$$

which makes the center of the average output state the same as that of the input state. Figure 9 also implies that when the ancillar squeezing becomes larger, the postselection scheme outperforms the feedforward scheme for the larger area of γ. However, it can be shown for a coherent state input that the feedforward scheme also works as the purity preserving transform in Eq. (21) when the electronic gain is set to be

$$g = \frac{(1 - e^{-2s})\sqrt{RT}}{(e^{-2s}R + T)}. \quad (24)$$

Therefore, the postselection scheme can perform interesting tasks which cannot be achieved by the feedforward scheme
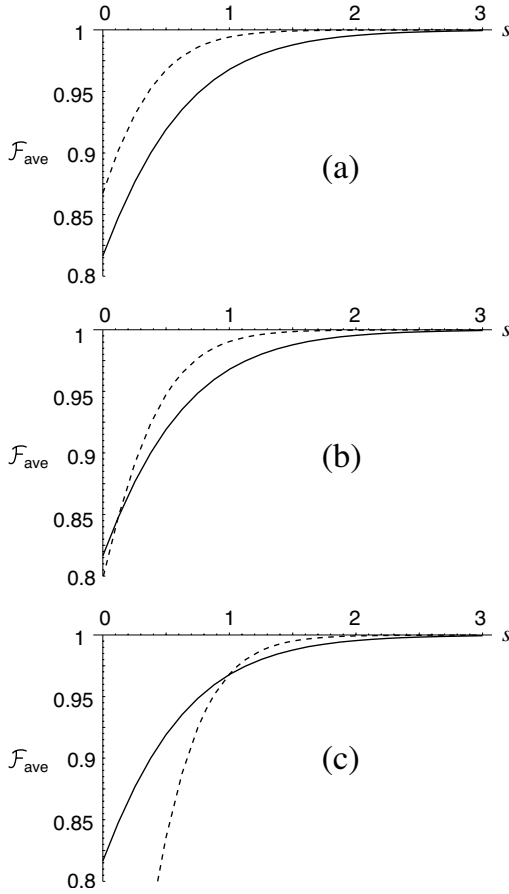
FIG. 9. The average fidelity $\mathcal{F}_{\text{ave}}$ between the output state from a coherent state input $|\gamma\rangle$ and an ideally squeezed coherent state by the feedforward scheme (solid line) and the post-selection scheme (dashed lime) against the ancillar squeezing s of the resource squeezed vacuum. $R=1/2$, $|X|<0.025$, and $s'=0.346574$. The coherent amplitudes are (a) $|\gamma|=0.5$, (b) $|\gamma|=1$, and (c) $|\gamma|=2$. The threshold for the postselection scheme is $x_0=0.025$.

for non-Gaussian inputs, while its transformation for Gaussian inputs can be achieved by a modification of the feedforward scheme [18].

III. EXPERIMENTAL DEMONSTRATION FOR COHERENT STATE INPUTS

As shown in the theoretical section, the postselection protocol is highly efficient for transforming both non-Gaussian input Fock states and Gaussian input coherent states. We experimentally demonstrated the principle of the postselection protocol using displaced coherent input states with realizable ancilla state squeezing. We characterized the efficacy of the postselection protocol by measuring the fidelity of postselected output state compared to the target state which is the ideal squeezed transform of the input state in the case of perfect ancillary state squeezing. For the experiment, the quantum states we considered reside at the sideband frequency (ω) of the electromagnetic field. Without the loss of generality, we denote the quadratures of these quantum states as $\hat{X}^\pm = \langle \hat{X}^\pm \rangle + \delta \hat{X}^\pm$, where $\langle \hat{X}^\pm \rangle$ are the quadrature expectation
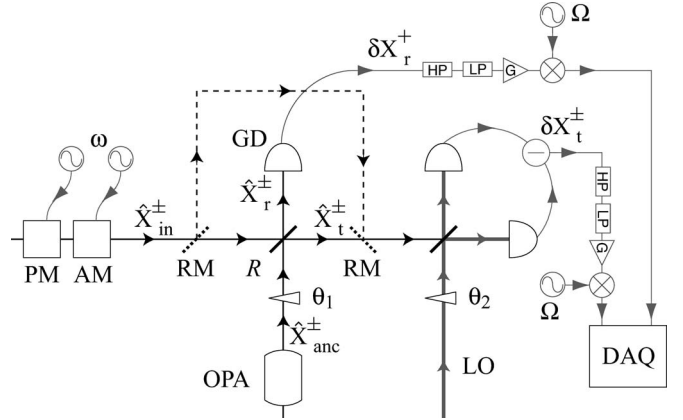

FIG. 10. (a) Schematic of the postselection protocol. $\hat{X}_{\text{in}}^\pm$: amplitude $(+)$ and phase $(-)$ quadratures of the input state; anc: ancilla state; r: reflected; t: transmitted; and out: postselected output state. R: beam-splitter reflectivity; GD: gate detector; RM: removable mirror; OPA: optical parametric amplifier; LO: local oscillator; AM/PM: amplitude/phase modulator; θ_1/θ_2: optical phase delay; HP/LP: high/low pass filters; G: radio frequency amplifier; ω: frequency of displaced coherent state at 6.81 MHz; Ω: electronic local oscillator at 6.875 MHz; DAQ: data acquisition system.

values, and where the quadrature variances are expressed by $V^\pm = \langle (\delta \hat{X}^\pm)^2 \rangle$.

Figure 10 shows the experimental setup for the postselection protocol. We used a hemilithic cavity MgO:LiNbO$_3$ below-threshold optical parametric amplifier, to produce an amplitude squeezed field at 1064 nm with a squeezing coefficient of $s=0.52\pm0.03$, corresponding to quadrature variances of $V_{\text{anc}}^+ = -4.5\pm0.2$ dB and $V_{\text{anc}}^- = +8.5\pm0.1$ dB with respect to the quantum noise limit. The amplitude squeezed state was a slightly mixed state due to decoherence as a result of losses in the optical parametric amplifier. More detail of this experimental production of squeezing is given in Ref. [19]. The displaced coherent states were produced at the sideband frequency of 6.81 MHz of the 1064 nm laser field using standard amplitude and phase electro-optic modulation techniques of the laser field [19]. To produce the phase squeezed ancillary state required in the protocol, the amplitude squeezed ancilla state $\hat{X}_{\text{anc}}^\pm$ was transformed to a phase squeezed state by interfering it with the displaced input coherent state $\hat{X}_{\text{in}}^\pm$, which had a much larger coherent amplitude, on the beam splitter (with reflectivity R) with a relative optical phase shift of $\pi/2$. This optical interference yielded two output states that were phase squeezed. The optical fringe visibility between the two fields was $\eta_{\text{vis}}=0.96\pm0.01$.

We directly detected the amplitude quadrature of the reflected state $\hat{X}_r^+$ using a detector, denoted by the gate detector in Fig. 10, which had a quantum efficiency of $\eta_{\text{det}}=0.92$ and an electronic noise of 6.5 dB below the quantum noise limit. The postselection process could, in principle, be achieved using an all optical setup, using an optical switch for example, but here we postselected *a posteriori* the quadrature measurements of the transmitted state $\hat{X}_{\text{tran}}^\pm$, which were measured using a balanced homodyne detector. The total homodyne detector efficiency was $\eta_{\text{hom}}=0.89$, with the electronic

noise of each detector 8.5 dB below the quantum noise limit. To characterize the protocol, for each experimental run we also measured the quadratures of the input displaced coherent state $\hat{X}_{\text{in}}^{\pm}$ using the same homodyne detector via a pair of removable mirrors (Fig. 10). To ensure accurate results, the total homodyne detector inefficiency was inferred out of all quadrature measurements for the postselected and input quantum states [19].

The electronic photocurrents of the detected quantum states (at a sideband frequency of 6.81 MHz) from the gate and homodyne detectors were electronically filtered, amplified, and demodulated down to 25 kHz using an electronic local oscillator at 6.785 MHz. The resulting photocurrents were digitally recorded using a NI PXI 5112 data acquisition system operating at a sample rate of 100 kS/s. Typically, 5 $\times 10^5$ (2×10^6) samples of data were taken for the $\hat{X}_{\text{in}}^{\pm}$ ($\hat{X}_t^{\pm}$ and $\hat{X}_r^{\pm}$) quadrature measurements, while 5×10^5 samples of data were taken for the noise calibration data. We used computational methods to apply a 25 kHz band-pass filter to the data centered at 25 kHz, removing technical noise at 0 Hz, and ensuring that the resulting frequency noise spectrum was homogenous. The data was demodulated to 0 Hz using a digital local oscillator at 25 kHz, and down-sampled to a sample rate of 25 kHz, so that it could be directly analyzed in the temporal domain.

We postselected the quadrature measurements of the transmitted state $\hat{X}_t^{\pm}$ which satisfied the threshold criteria $|X_r^+| < x_0$. The postselection threshold was dependent on the beam-splitter reflectivity used in the protocol. For a beam-splitter reflectivity of $R=0.75$ and $R=0.5$ we used an experimentally optimized threshold of $x_0=0.009$ and $x_0=0.005$ respectively. Hence, the postselection threshold was independent of the input state, but dependent on the beam-splitter reflectivity.

We characterized the efficacy of the postselection protocol as an ideal single mode squeezer, by determining the fidelity of the postselected output state with a target state that is an ideal squeezed operation of the input state [Eq. (21)]. The Wigner function of the ideal squeezed input state is given by $W_{\text{out}}(\gamma; s')$, where $s \to \infty$ and $s' \to -\ln[T]/2$. In this case, the fidelity is given by $\mathcal{F}(X_r^+) \pi \int_{-\infty}^{\infty} d^2 \gamma W_{\text{expt}}(\gamma; X_r^+) W_{\text{out}}(\gamma; s')$, where $W_{\text{expt}}(\gamma; X_r^+)$ is the Wigner function of the postselected output state. From this expression the average fidelity $\mathcal{F}_{\text{ave}}$ for a postselection threshold x_0 can be calculated. This corresponds to unity fidelity $\mathcal{F}_{\text{ave}}=1$ in the limit of ideal ancilla state squeezing and $X_r^+=0$. In the experiment, the input state was not coherent, but rather a slightly mixed state due to inherent low-frequency classical noise on the laser beam, with quadrature variances of $V_{\text{in}}^+=1.13\pm0.02$ and $V_{\text{in}}^-=1.05\pm0.02$, with respect to the quantum noise limit. Hence, we calculated the fidelity with respect to the ideal squeezing transform of the experimental input state. Figure 11 shows the classical fidelity limit, in the case where the ancilla squeezed state is replaced with a vacuum state. The classical fidelity limit $\mathcal{F}_{\text{clas}}$, is maximized by considering additional classical noise on the phase quadrature of the input vacuum state (Fig. 11). Exceeding this classical fidelity limit can only be achieved using quantum resources.

Figure 11 shows the experimental fidelity for varying amplitude quadrature expectation values of the input states
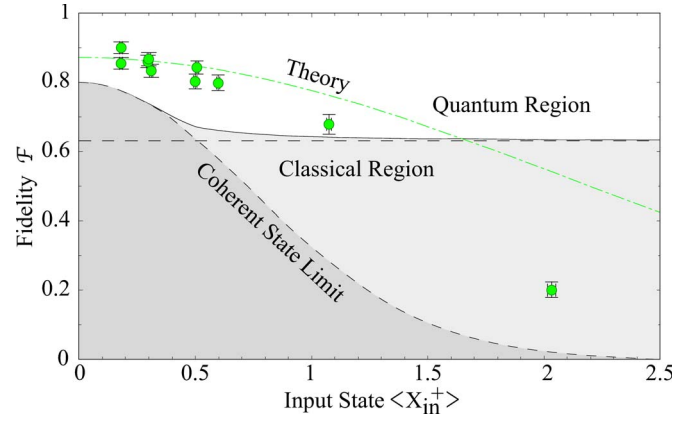

FIG. 11. (Color online) Experimental fidelity of the postselected output state for varying amplitude quadrature expectation values of the input coherent state $|\gamma^+| \equiv \langle \hat{X}_{\text{in}}^+ \rangle$, for $R=0.75$ and $x_0=0.009$. Dark grey region: classical fidelity limit for an ancilla vacuum state, Light grey region: classical fidelity limit. Dot-dashed line: calculated theoretical curve including experimental losses and the finite postselection threshold.

$|\gamma^+| \equiv |\langle \hat{X}_{\text{in}}^+ \rangle|$. We point out that for the majority of the input states, both the amplitude and phase quadrature expectation values were approximately equal with $\langle \hat{X}_{\text{in}}^+ \rangle \approx \langle \hat{X}_{\text{in}}^- \rangle$. For a beam-splitter reflectivity of $R=0.75$, we achieved a best fidelity of $\mathcal{F}_{\text{ave}}=0.90\pm0.02$ for an input state $\langle \hat{X}_{\text{in}}^+ \rangle=0.18\pm0.01$, which exceeds the maximum classical fidelity of $\mathcal{F}_{\text{clas}}=4/5=0.8$ (see Fig. 12). This postselected output state had quadrature variances of $V_{\text{out}}^+=4.70\pm0.11$ and $V_{\text{out}}^-=0.51\pm0.01$. The mean quadrature displacement gains $g^{\pm}=\langle \hat{X}_{\text{out}}^{\pm} \rangle / \langle \hat{X}_{\text{in}}^{\pm} \rangle$, which measure the ratio of the quadrature expectation values of the postselected output state with respect to the input state, were measured to be $g^+=0.71\pm0.16$ and $g^-=0.50\pm0.06$. This is compared with the ideal case of perfect ancilla state squeezing and a postselection threshold of $\hat{X}_r^+=0$, where the ideal theoretical gains are $g_{\text{ideal}}^+=2$ and $g_{\text{ideal}}^-=1/2$. The phase gain was controlled by the beam-
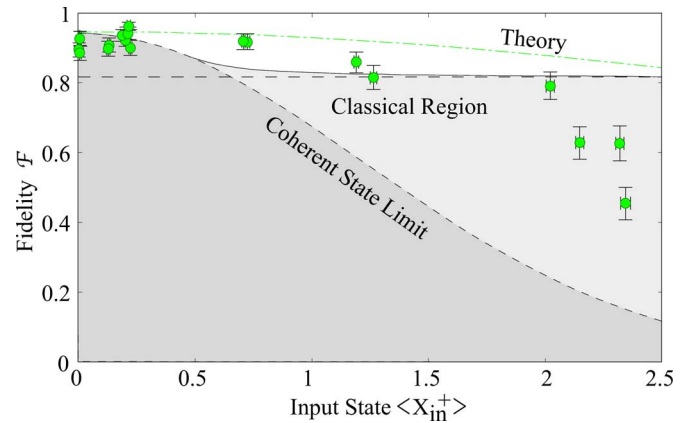

FIG. 12. (Color online) Experimental fidelity of the postselected output state for varying amplitudes $\langle \hat{X}_{\text{in}}^+ \rangle$ of the input coherent state, for $R=0.75$ and $x_0=0.009$.
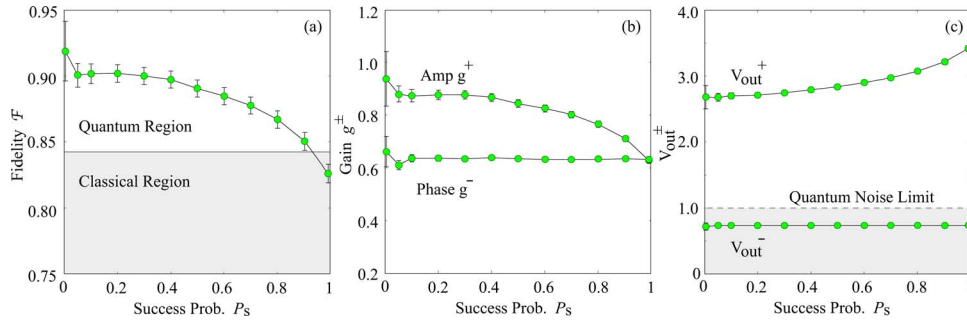
FIG. 13. (Color online) (a) Experimental fidelity of the postselected output state for varying success probability corresponding to varying postselection threshold. $R=0.5$ and $\langle \hat{X}^+_{in} \rangle = 0.71$. Light grey region: classical fidelity region. (b) Experimental optical quadrature gains $g^\pm = \langle \hat{X}^\pm_{out} \rangle / \langle \hat{X}^\pm_{in} \rangle$ for varying success probability. (c) Experimental quadrature variances of the postselected output state $V^\pm_{out}$ for varying success probability.

splitter transmittivity, while the amplitude gain was less than the ideal case due to finite ancilla state squeezing, finite postselection threshold and experimental losses. The quantum nature of the postselection protocol is demonstrated by the experimental fidelity results that exceed the classical fidelity limit in Fig. 11. For large input states $\langle \hat{X}^+_{in} \rangle$, the experimental fidelity was less than the theoretical prediction due to electronic detector noise and the finite resolution of the data acquisition system, resulting in a smaller postselected output state $\langle \hat{X}^+_{in} \rangle$ and a corresponding decrease in the experimental fidelity.

Figure 13(a) illustrates how the experimental fidelity of a postselected state transitions from the classical to the quantum fidelity region by decreasing the postselection threshold and corresponding probability of success. Figure 13(b) shows how the corresponding mean amplitude quadrature displacement gain g^+ increases as a result of this process, while the phase gain remains approximately unchanged. Similarly, Fig. 13(c) shows how the amplitude quadrature variance of the postselected state V^+_{out} is reduced, whilst the phase quadrature variance V^-_{out} remains approximately unchanged, as the postselection threshold is decreased

We also characterized the experiment in terms of the purity of the postselected output state, defined as $\mathcal{P} = tr(\rho^2_{out})$. In the case of Gaussian states, the purity of the output state can be expressed as $\mathcal{P} = (V^+_{out} V^-_{out})^{-1/2}$. In the ideal case of a lossless experiment and a postselection threshold $X^+_r = 0$, the protocol is a purity preserving transform, independent of the input state and the amount of squeezing of the ancilla state. In the experiment, as the input states were slightly mixed, we calculated the purity of the postselected output state, normalized to the purity of the input state, which is given by $\mathcal{P}_{norm}(V^+_{out} V^-_{out})^{-1/2}/(V^+_{in} V^-_{in})^{-1/2}$. Figure 14(a) shows the experimental purity of the postselected output state for varying input states, which illustrates how the purity is improved via the postselection process. For a beamsplitter reflectivity of $R=0.75$ we achieved a best purity of $\mathcal{P}_{norm} = 0.81 \pm 0.04$ for an input state of $\langle \hat{X}^+_{in} \rangle = 2.03 \pm 0.02$. Figure 14(a) shows that the purity of the postselected output states were approximately independent of the input states, for a large range of input states.

We also implemented the postselection scheme for a beam-splitter reflectivity of $R=0.5$. In this case, we measured

a best fidelity of $\mathcal{F}_{ave} = 0.96 \pm 0.01$, which exceeded the maximum classical fidelity of $\mathcal{F}_{clas} = \sqrt{8/3} \approx 0.94$ as shown in Fig. 12. We measured a best experimental normalized purity of $\mathcal{P}_{norm} = 0.80 \pm 0.04$ which is shown in Fig. 14(b).

IV. REMARKS

We have investigated a continuous-variable conditioning scheme based on a beam-splitter interaction, homodyne detection, and an ancilla squeezed vacuum state [9]. It transforms input Fock states to squeezed single photons and SCSs, which have applications in the field of quantum information, with realizable squeezing of the ancilla state [9]. We have found that an SCS with well defined parity and high fidelity can be generated from a Fock state of $n \leq 4$, and we conjecture that this can be generalized for an arbitrary n. Further, for Gaussian coherent states, this technique provides an alternative to continuous electro-optic feedforward schemes. The postselection scheme provides an interesting transformation for coherent states which results in higher fidelities to the ideal squeezing operation when amplitudes are small. All the interesting features of the postselection scheme for non-Gaussian inputs discussed in this paper *cannot* be achieved using the feedforward method in Ref. [17]. We
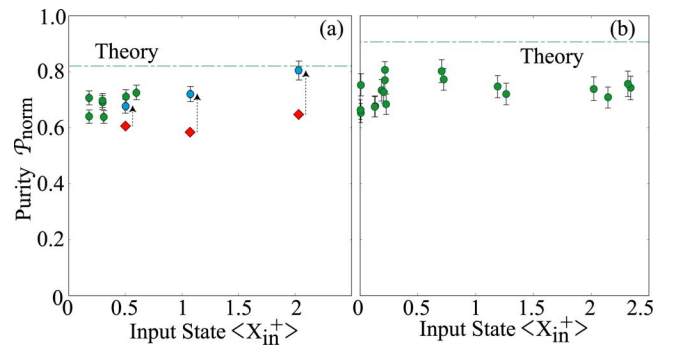

FIG. 14. (Color online) (a) Experimental normalized purity for varying input states $\langle \hat{X}^+_{in} \rangle$, for $R=0.75$ and $x_0 = 0.009$. Dash arrows show purity prior to (diamonds) and after (circles) postselection. Dot-dashed line: calculated theoretical prediction of the experiment. (b) Experimental purity for varying input state $\langle \hat{X}^+_{in} \rangle$, for $R=0.5$ and $x_0 = 0.005$.

have described, in detail, the experimental demonstration of the principles of this scheme using coherent states, where fidelities were measured that are only achievable using quantum resources [9].

[1] M. Nielsen and I. Chuang, *Quantum Computation and Quantum Information* (Cambridge University Press, Cambridge, UK, 2000).

[2] J. L. O'Brien, G. J. Pryde, A. G. White, T. C. Ralph, and D. Branning, Nature (London) **426**, 264 (2003).

[3] E. Knill, R. Laflamme, and G. J. Milburn, Nature (London) **409**, 46 (2001).

[4] M. Dakna, J. Clausen, L. Knöll, and D.-G. Welsch, Phys. Rev. A **59**, 1658 (1999); J. Clausen, M. Dakna, L. Knöll, and D.-G. Welsch, Opt. Commun. **179**, 189 (2000).

[5] M. G. A. Paris, M. Cola, and R. Bonifacio, Phys. Rev. A **67**, 042104 (2003).

[6] J. Laurat, T. Coudreau, N. Treps, A. Maitre, and C. Fabre, Phys. Rev. Lett. **91**, 213601 (2003).

[7] S. A. Babichev, B. Brezger, and A. I. Lvovsky, Phys. Rev. Lett. **92**, 047903 (2004).

[8] T. C. Ralph, A. P. Lund, and H. M. Wiseman, J. Opt. B: Quantum Semiclassical Opt. **7**, S245 (2005).

[9] A. M. Lance, H. Jeong, N. B. Grosse, T. Symul, T. C. Ralph, and P. K. Lam, Phys. Rev. A **73**, 041801(R) (2006).

[10] H. Jeong, M. S. Kim, and J. Lee, Phys. Rev. A **64**, 052308 (2001); T. C. Ralph, A. Gilchrist, G. J. Milburn, W. J. Munro, and S. Glancy, *ibid.* **68**, 042319 (2003).

[11] E. Schrödinger, Naturwiss. **23**, 807 (1935); **23**, 823 (1935); **23**, 844 (1935).

[12] A. P. Lund, H. Jeong, T. C. Ralph, and M. S. Kim, Phys. Rev. A **70**, 020101(R) (2004); H. Jeong, A. P. Lund, and T. C. Ralph, *ibid.* **72**, 013801 (2005).

[13] J. Wenger, R. Tualle-Brouri, and P. Grangier, Phys. Rev. Lett. **92**, 153601 (2004).

[14] J. S. Neergaard-Nielsen, B. M. Nielsen, C. Hettich, K. Mölmer, and E. S. Polzik, quant-ph/0602198 (unpublished).

[15] S. Olivares and M. G. A. Paris, J. Opt. B: Quantum Semiclassical Opt. **7**, S616 (2005).

[16] S. Suzuki, K. Tsujino, F. Kannari, and M. Sasaki, Opt. Commun. **259**, 758 (2006).

[17] R. Filip, P. Marek, and U. L. Andersen, Phys. Rev. A **71**, 042308 (2005); P. K. Lam, T. C. Ralph, E. H. Huntington, and H.-A. Bachor, Phys. Rev. Lett. **79**, 1471 (1997).

[18] J. Fiurasek, R. Garcia-Patron, and N. J. Cerf, Phys. Rev. A **72**, 033822 (2005).

[19] W. P. Bowen, N. Treps, B. C. Buchler, R. Schnabel, T. C. Ralph, Hans-A. Bachor, T. Symul, and P. K. Lam, Phys. Rev. A **67**, 032302 (2003); A. M. Lance, T. Symul, W. P. Bowen, B. C. Sanders, and P. K. Lam, Phys. Rev. Lett. **92**, 177903 (2004).